Title	A Unified Reduced Order Model for Standing Balance Captures Biological Balance Strategy Preferences
Author(s)	Huckell, Thomas; Wu, R. Amy
Citation	The 9.5th International Symposium on Adaptive Motion of Animals and Machines (AMAM2021). 2021, p. 23
Version Type	VoR
URL	https://doi.org/10.18910/84864
rights	
Note	

A Unified Reduced Order Model For Standing Balance Captures Biological Balance Strategy Preferences

Thomas Huckell[a], Amy R. Wu[a]
[a]Ingenuity Labs Research Institute, Department of Mechanical and Materials Engineering,
Queen's University, Kingston ON, Canada
thomas.huckell@queensu.ca, amy.wu@queensu.ca

1 Introduction

Legged robots have the potential to transform society by traversing remote or dangerous areas or by performing tedious locomotor tasks. Much like humans, legged robots need to compensate and adjust for unintended disturbances through active balancing to maintain stability. Both human and robot balancing have been primarily grouped into discrete strategies: ankle, hip, toe and stepping [1,2]. The ankle strategy uses ankle torques to position the center of pressure (CoP). The hip strategy uses upper body dynamics to generate angular momentum about the center of mass (CoM). The toe strategy uses vertical CoM dynamics to modulate the ground reaction force. Here we focus on standing balance strategies without stepping.

These three balancing strategies can be approximated by reduced order models. The linear inverted pendulum (LIP) model consists of a point mass supported by a massless leg [3], leading to a linear system that can be controlled through CoP positioning, modelling the ankle strategy. The hip strategy can be modeled with the linear inverted pendulum plus flywheel (LIPPFW) model which adds a flywheel with inertial properties to the LIP model [4]. The toe strategy can be captured by the variable height inverted pendulum (VHIP) model where the vertical CoM dynamics allow for regulation of the ground reaction force magnitude [5]. In this study, we aimed to elucidate the relative contributions of these three balancing strategies, both separately and within an unified model, by comparing the performance of the reduced order models in a zero step push recovery simulation.

2 Methods

To evaluate push recovery performance, we used trajectory optimization with the reduced order models to determine the optimal control strategy.

2.1 Reduced Order Models

The unified model, which we term the variable height inverted pendulum model plus flywheel (VHIPPFW) model, includes LIP, flywheel, and vertical dynamics. Its sagittal dynamics and flywheel dynamics are given by Eq. (1) and (2) respectively.

$$\ddot{x} = \frac{g+\ddot{z}}{z}(x-x_c) - \frac{\tau}{mz} \tag{1}$$

$$I\ddot{\theta} = \tau \tag{2}$$

where x is the horizontal CoM position, g is gravitational acceleration, z is the vertical CoM position, x_c is the CoP position, τ is the flywheel torque, m is the mass, θ is the flywheel angle, and I is the flywheel inertia. We defined $X = [x,\theta,z,\dot{x},\dot{\theta},\dot{z}]^T$ and $U = [x_c,\tau,\ddot{z}]^T$ as the state and control input vectors, respectively. When $\ddot{z}$ is zero, τ is zero, or both are zero, the unified model reduces to the LIPPFW [6], VHIP [5], and LIP models [3], respectively.

2.2 Trajectory Optimization

Trajectory optimization was used to determine the set of controls that minimize the deviation from the rest state and the total cost of control. The optimal trajectory was computed using a trapezoidal direct collocation method [7] and minimized an objective function J that was designed to equally penalize the state X's deviation from the rest state X_0 and equally penalize the control cost. We used weighting matrices to normalize the state position and control components to their respective upper bounds and each state velocity component by the maximum velocity experienced during the largest recoverable disturbance. The objective function is given by Eq. (3),

$$J = \sum_{i}^{N} \tilde{X}_i^T Q \tilde{X}_i + U_i^T R U_i, \tag{3}$$

where $\tilde{X}_i = X_i - X_0$, $Q = \text{diag}(x_{c_{max}}^{-2}, \theta_{max}^{-2}, (z_{max} - z_0)^{-2}, 0.42^{-2}, 2.3^{-2}, 0.44^{-2})$ and $R = \text{diag}(U_{max}^{-2})$ are the weighing matrices, and N is the number of knot points. For our simulation, we used $N = 40$.

2.3 Push Recovery Simulation

We applied pushes to the four reduced order models with mass of $m = 80$ kg and flywheel inertia of $I = 10$ kg-m^2 (state and control bounds in Tab. 1). The push disturbance was modeled as a constant horizontal force applied at the CoM for a duration of 0.1 s. The simulation started with the model at rest at a height of 1 m with the CoM centered over the base of support. A range of push force magnitudes were
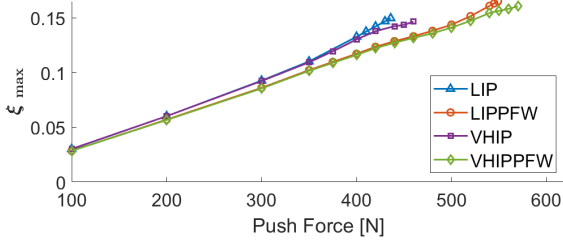
Figure 1: Maximum capture point ξ_{max} of the four balancing models during push recovery.

Figure 2: Percent contribution of each control strategy using normalized control cost of the VHIPPFW model.

applied to the individual models with increased resolution as each model approached their recovery limits. Push recovery performance was evaluated by the maximum capture point ξ_{max} experienced. The capture point is given by Eq. (4),

$$\xi = x + \omega^{-1}\dot{x}, \tag{4}$$

where $\omega^2 = g/z$. As one metric of stability [6], ξ represents the CoP location for the LIP model's passive dynamics to bring the system back to rest [4]. Increased values of ξ indicate larger excursions of CoM position and velocity.

Table 1: Model state and control bounds.

Symbol	Description	Rest	Min	Max
θ	flywheel angle(rad)	0	$-\frac{\pi}{6}$	$\frac{\pi}{4}$
z	CoM height (m)	1	0.9	1.1
x_c	CoP position (m)	0	-0.15	0.15
τ	flywheel torque (Nm)	0	-80	80
$\ddot{z}$	vertical acceleration (m/s^2)	0	-3	3

3 Results

The maximum push force that each model can recover from was 436 N (LIP), 462 N (VHIP), 549 N (LIPPFW), and 570 N (VHIPPFW). For a given push ξ_{max} was the smallest in VHIPPFW followed by LIPPFW, VHIP and LIP (Fig 1) making VHIPPFW the most stable. There were two ξ_{max} trends, one between the LIP and VHIP and the other between the LIPPFW and VHIPPFW, and each trend separated when the push forces approached each model's respective stability limits.

To identify the relative contributions of each strategy during push recovery, we compared the normalized cost of each control component in the unified VHIPPFW model as a percentage of the total normalized cost. We found that ankle control was the dominant strategy with x_c control accounting for greater than 96.0% of the total control cost for pushes less than 300 N (Fig 2). For pushes greater than 400 N, the ankle strategy dropped while the hip increased in compensation. As pushes exceed 520 N, the hip strategy started to decrease while the toe began to increase. At the recovery limit of 570 N, the hip and toe strategies accounted for 26.6 and 14.5 % of the total control cost respectively.
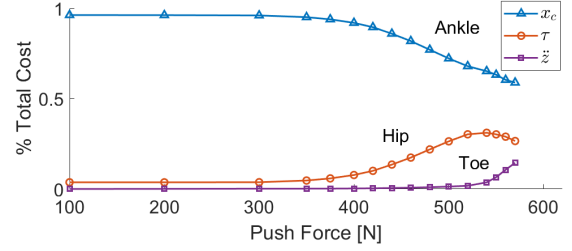
4 Discussion

We simulated push recovery on four reduced order models that embodied different biological balancing strategies using trajectory optimization. We found that the ankle strategy is preferred while hip and toe strategies are applied in a hierarchical manner, only being employed when the former strategy approaches its limits. The unified model parallels the preference in human balance strategies from ankle to hip with increasing applied perturbation magnitudes [2].

The scope of our study is currently limited to considering one push profile (duration, direction) and one set of bounds for the state and control. However, parameters used in our simulation were chosen to approximate a humanoid biped to deliver insights on the effectiveness of each balancing strategy if they were to be implemented as a unified strategy in hardware. Thus, we believe that the overall relative performance among the four models would still hold with varied push profiles. The combination of human-like balance strategies, modelled with reduced order models, naturally reveal human-like preferences to push recovery, yielding promising directions for robust balance control for legged robots.

5 Acknowledgments

References

[1]   C. McGreavy, K. Yuan, D. Gordon, K. Tan, W. J. Wolfslag, S. Vijayakumar, and Z. Li, "Unified push recovery fundamentals: Inspiration from human study," in *Proc. 2020 IEEE ICRA*, 2020.

[2]   A. Hof, "The equations of motion for a standing human reveal three mechanisms for balance," *J Biomech*, vol. 40, no. 2, pp. 451–457, 2007.

[3]   S. Kajita, F. Kanehiro, K. Kaneko, K. Yokoi, and H. Hirukawa, "The 3D linear inverted pendulum mode: a simple modeling for a biped walking pattern generation," in *Proc. 2001 IEEE/RSJ IROS*, vol. 1, pp. 239–246 vol.1, Oct. 2001.

[4]   J. Pratt, J. Carff, S. Drakunov, and A. Goswami, "Capture point: A step toward humanoid push recovery," in *2006 6th IEEE-RAS International Conference on Humanoid Robots*, pp. 200–207, 2006.

[5]   B. J. van Hofslot, R. Griffin, S. Bertrand, and J. Pratt, "Balancing Using Vertical Center-of-Mass Motion: A 2-D Analysis From Model to Robot," *IEEE Robot. and Autom. Lett.*, vol. 4, pp. 3247–3254, Oct. 2019.

[6]   B. Stephens, "Humanoid push recovery," in *2007 7th IEEE-RAS Int. Conf. on Humanoid Robots*, pp. 589–595, Nov. 2007.

[7]   M. Kelly, "An Introduction to Trajectory Optimization: How to Do Your Own Direct Collocation," *SIAM Rev.*, vol. 59, pp. 849–904, Jan. 2017.